Supporting Information for

Spin Texture Evolution of Rashba Splitting under Pressure: A Case Study of Inorganic Nitride Perovskite Crystal

Showkat H. Mir[†] and Sudip Chakraborty[*,‡]

†*Materials Theory for Energy Scavenging (MATES) Lab, Harish-Chandra Research Institute (HRI) Allahabad, A CI of Homi Bhabha National Institute (HBNI), Chhatnag Road, Jhunsi, Prayagraj (Allahabad) 211019 India.*

‡[a]*Materials Theory for Energy Scavenging (MATES) Lab, Harish-Chandra Research Institute (HRI) Allahabad, A CI of Homi Bhabha National Institute (HBNI), Chhatnag Road, Jhunsi, Prayagraj (Allahabad) 211019 India.*

E-mail: sudiphys@gmail.com;sudipchakraborty@hri.res.in

Computational Methodology

The density functional theory (DFT)[1,2] calculations were performed using Vienna Ab-initio Simulation Package (VASP),[3] and the supplied PAW pseudo-potentials with Perdew-Burke-Ernzerhof generalized gradient approximation (GGA).[4] The potential for Ce and Ta included the semi-core d and p orbitals in the valence states, respectively. Thus, the valence configuration for Ce, Ta, and N atoms were $3d^{10}4f^{1}5d^{1}$, $5p^{6}6s^{2}5d^{3}$ and $2s^{2}2p^{3}$, respectively. The

optimization process, band structure, density of states (DOS), and spin texture calculations were performed with SOC included. The full cell lattice parameters and relaxation of internal atomic positions were performed using a $9 \times 9 \times 6$ k-point mesh containing the Γ-point, and DOS was calculated using a $12 \times 12 \times 8$ mesh. A converged cutoff energy of 450 eV (Figure S1) was employed in all calculations. For the structural optimization, the change in total energy between two ionic relaxation steps was smaller than 10^{-7} eV, and the residual force on each ion was less than 0.001 eV/Å. Ferroelectric polarization has been evaluated using the modern theory (Berry-phase theory) of polarization. Phonon dispersion was calculated using the density functional perturbation theory.[5,6] Both Ferroelectric polarization and phonon dispersion were computed using the Quantum-ESPRESSO package.[5] We plotted spin textures using MCU[7] and pyprocar[8] codes.

Formation energy (E_f) was calculated using elemental reference energies in the equation

$$E_f = E_{\mathrm{CeTaN_3}} - E_{Ce} - E_{Ta} - E_N \tag{1}$$

where $E_{\mathrm{CeTaN_3}}$ is the ground state total energy of the perovskite phase and E_{Ce}, E_{Ta}, and E_N are the energies of Ce, Ta, and N bulk phases, respectively. To calculate the elemental energies, we considered as reference their most stable structures reported in the Materials Project database.[9] We used the finite difference method to obtain the Hessian matrix to calculate elastic constants. In this approach, displacements of every ion are made in the direction of each Cartesian coordinate in the lattice, and the Hessian is determined from the atomic displacements.[10] The elastic tensor is then calculated by distorting the original lattice, and the desired elastic constants are derived using the strain-stress relationship.[11]

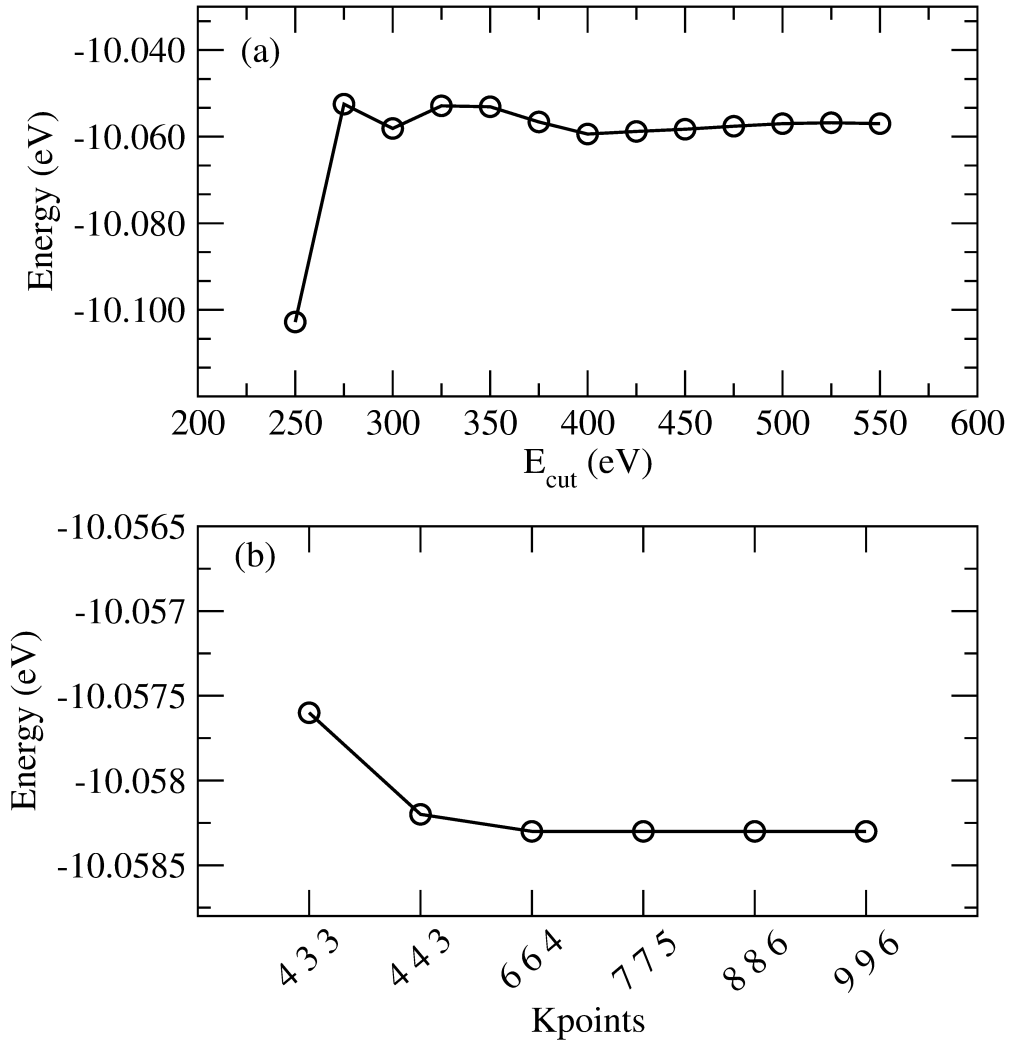

Figure S1: Energy plotted as a function of cutoff energy (E_{cut}) and K-points to determine the converged values of E_{cut} and K-grid. From (a), we used the E_{cut} 450 eV, and (b) indicates that energy converges after 6 6 4 K-point grid.

Table S1: Calculated energy (PBE+SOC.) and materials project id for some decomposition compounds considered in the present work. The calculated energy of $CeTaN_3$ is also included in the table

Compound	Materials Project-id	Energy on Convex hull (E_h)	Energy/fu (eV)
$Ce_2(TaN_3)_2$	867221	0	109.111
CeN	293	0	-17.632
Ta_3N_5	27488	0	-87.458
Ta_5N_6	1642	0	-124.852
TaN	1279	0	-23.166
Ta_2N	107938	0	-36.177
$CeTaN_3$	-	-	-50.291
N_2(g)	-	-	-14.867

Table S2: Calculated elastic constants (GPa) of CeTaN3 in orthorhombic phase using PBE+SOC.

C_{11}	C_{22}	C_{33}	C_{44}	C_{55}	C_{66}	C_{12}	C_{13}	C_{23}
359.07	340.0	410.16	103.40	138.39	124.01	140.33	15.98	141.32

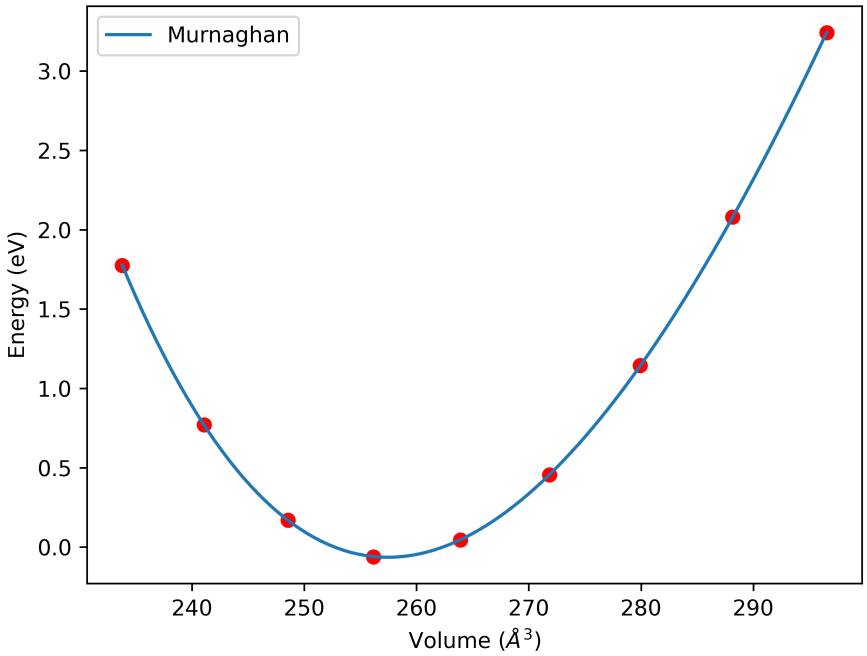

Figure S2: Energy as a function of volume. By fitting Murnaghan[12] EOS to energy vs. volume data, we obtained a Bulk Modulus of 228.03 GPa for $CeTaN_3$. Red circles denote the calculated values, and the blue line represents the fitted line. The large bulk modulus indicates high resistance to external stress.

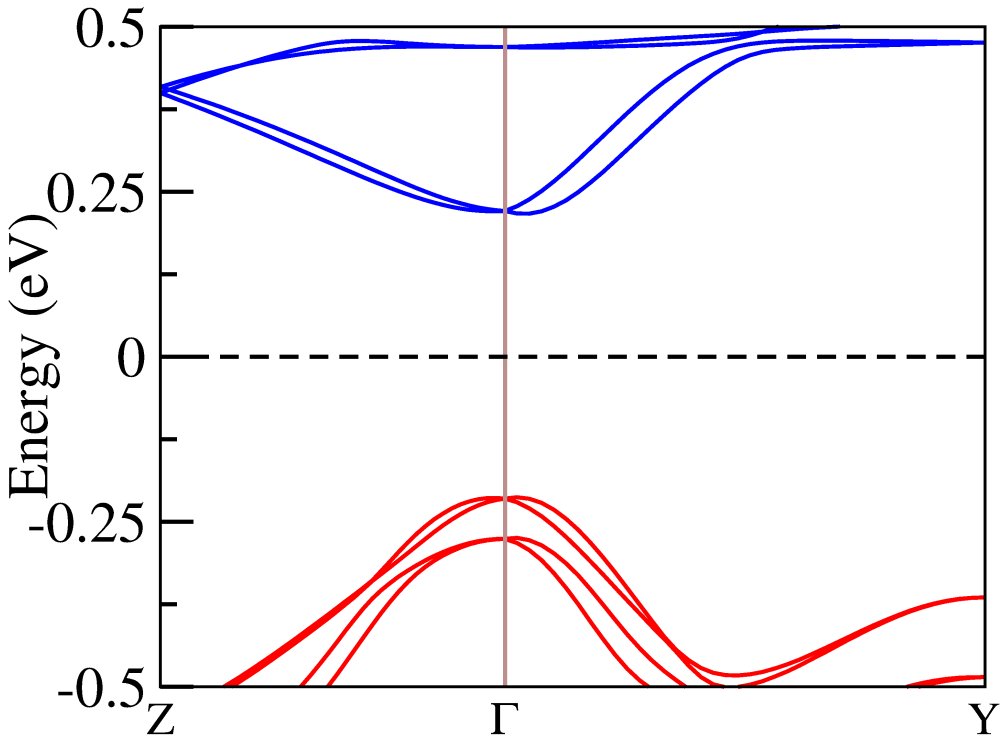

Figure S3: SOC band structure. Both CBM and VBM are offset from the Γ-point due to which direct band gap nature is preserved

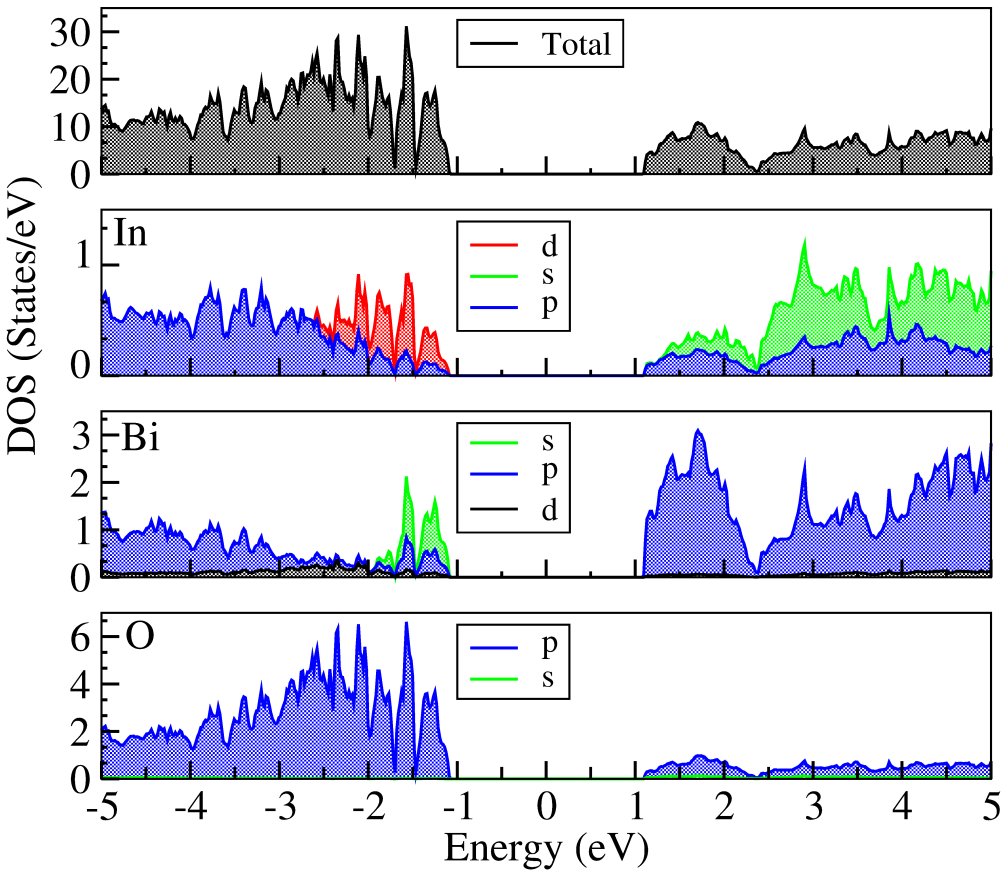

Figure S4: Total and projected DOS of $BiInO_3$ with SOC included.

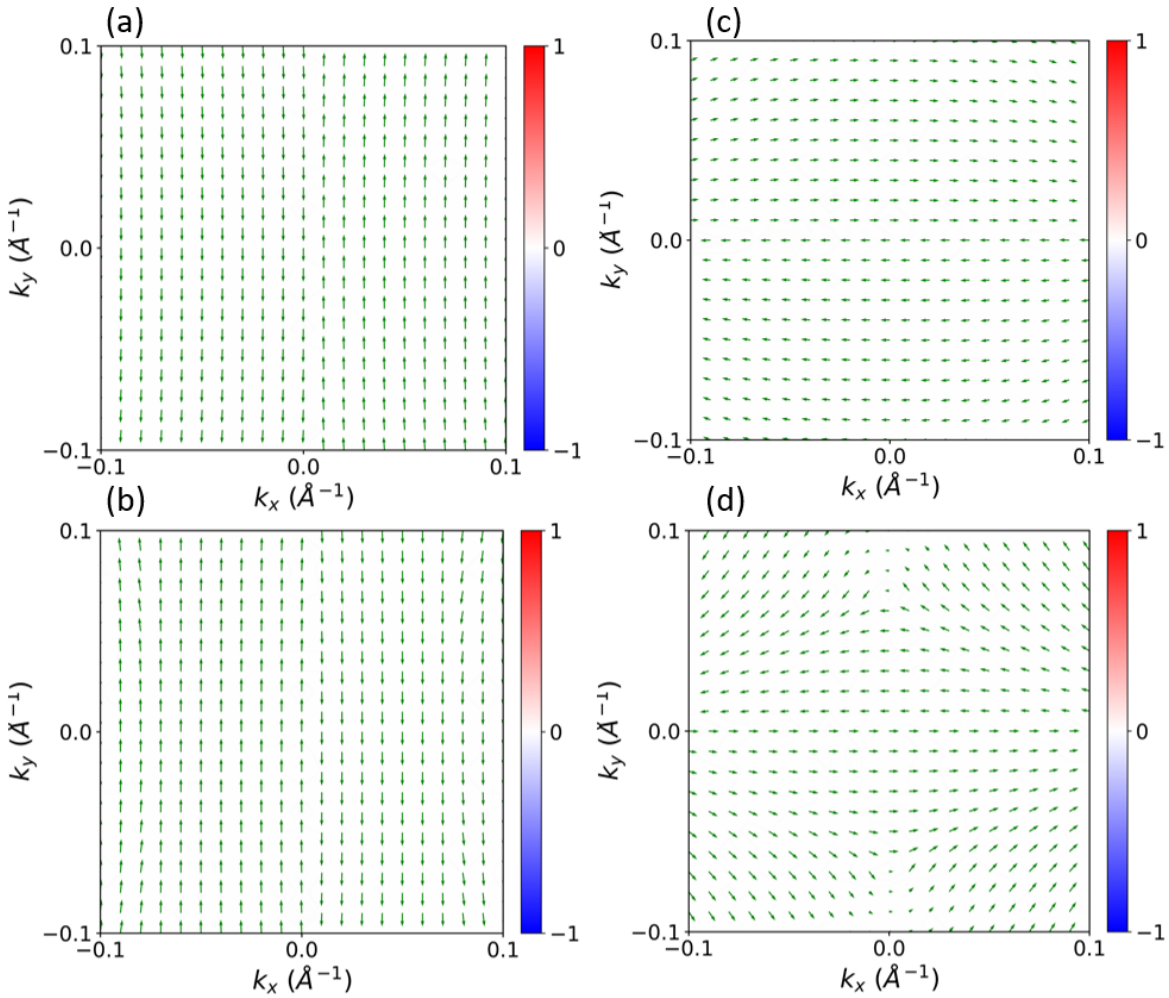

Figure S5: Spin texture of $BiInO_3$ at symmetry points X and Y of the Brillouin zone. (a) Outer (b) inner branch at Point X, (c) Outer (d) inner branch at Point Y. The green arrows denote in-plane spin texture. The color bar denotes the out-of-plane spin texture. From (a-d), it is clear that there is no out-of-plane spin component.

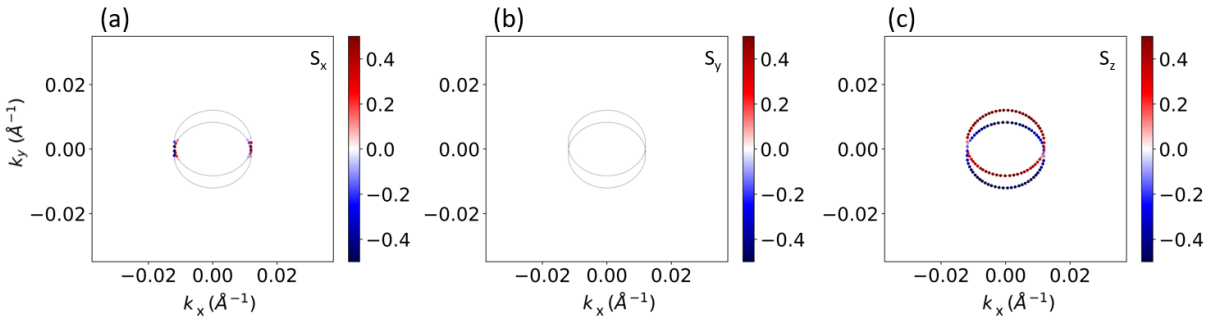

Figure S6: Spin texture plotted for valence band of $CeTaN_3$ around symmetry point Γ of the Brillouin zone at 0 GPa. Constant energy contours (a) – (c) show Sx, Sy, and Sz spin components in the valence band at -0.25 eV below the Fermi energy. The color scale shows the up and down spin components.

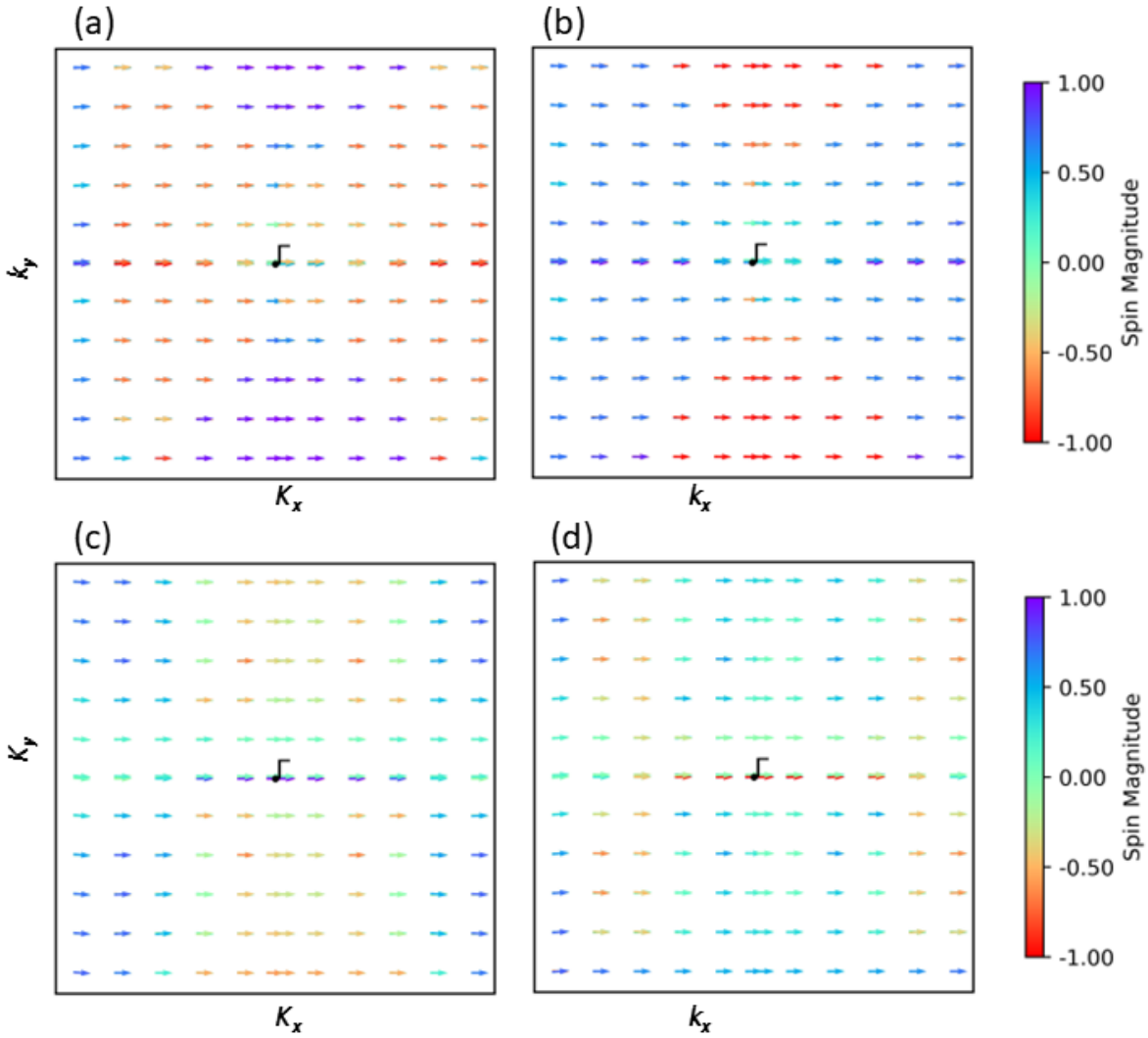

Figure S7: Spin texture plotted for conduction band minimum and valence band maximum of $CeTaN_3$ at symmetry point Y of the Brillouin zone at 0 GPa. (a) and (b) inner branch and outer branches of the valence band, (c) and (d) inner branch of the conduction band. The arrows denote in-plane spin texture and the color of the arrows signifies the spin component in the perpendicular direction (z-axis). Nota bene: This type of spin texture was plotted using vaspkit.[13]

References

(1) Hohenberg, P.; Kohn, W. Inhomogeneous electron gas. *Physical review* **1964**, *136*, B864.

(2) Kohn, W.; Sham, L. J. Self-consistent equations including exchange and correlation effects. *Physical review* **1965**, *140*, A1133.

(3) Kresse, G.; Furthmüller, J. Efficient iterative schemes for ab initio total-energy calculations using a plane-wave basis set. *Phys. Rev. B* **1996**, *54*, 11169–11186.

(4) Blöchl, P. E. Projector augmented-wave method. *Phys. Rev. B* **1994**, *50*, 17953–17979.

(5) Giannozzi, P.; Baroni, S.; Bonini, N.; Calandra, M.; Car, R.; Cavazzoni, C.; Ceresoli, D.; Chiarotti, G. L.; Cococcioni, M.; Dabo, I.; others QUANTUM ESPRESSO: a modular and open-source software project for quantum simulations of materials. *Journal of physics: Condensed matter* **2009**, *21*, 395502.

(6) Mir, S. H. Exploring the electronic, charge transport and lattice dynamic properties of two-dimensional phosphorene. *Physica B: Condensed Matter* **2019**, *572*, 88–93.

(7) Pham, H. MCU: Modeling and Crystallographic Utilities. 2023; `https://github.com/hungpham2017/mcu`.

(8) Herath, U.; Tavadze, P.; He, X.; Bousquet, E.; Singh, S.; Muñoz, F.; Romero, A. H. PyProcar: A Python library for electronic structure pre/post-processing. *Computer Physics Communications* **2020**, *251*, 107080.

(9) Jain, A.; Ong, S. P.; Hautier, G.; Chen, W.; Richards, W. D.; Dacek, S.; Cholia, S.; Gunter, D.; Skinner, D.; Ceder, G.; others Commentary: The Materials Project: A materials genome approach to accelerating materials innovation. *APL materials* **2013**, *1*, 011002.

(10) Olsson, E.; Aparicio-Anglès, X.; de Leeuw, N. H. A DFT+ U study of the structural, electronic, magnetic, and mechanical properties of cubic and orthorhombic $SmCoO_3$. *The Journal of chemical physics* **2016**, *145*, 224704.

(11) Roldan, A.; Santos-Carballal, D.; de Leeuw, N. H. A comparative DFT study of the mechanical and electronic properties of greigite Fe3S4 and magnetite Fe_3O_4. *The Journal of Chemical Physics* **2013**, *138*, 204712.

(12) Murnaghan, F. D. The compressibility of media under extreme pressures. *Proceedings of the National Academy of Sciences* **1944**, *30*, 244–247.

(13) Wang, V.; Xu, N.; Liu, J.-C.; Tang, G.; Geng, W.-T. VASPKIT: A user-friendly interface facilitating high-throughput computing and analysis using VASP code. *Computer Physics Communications* **2021**, *267*, 108033.